2004-01-2405

Mesoporous Oxide Supported Catalysts for Low Temperature Oxidation of Dissolved Organics in Spacecraft Wastewater Streams

James R. Akse and John T. Holtsnider
UMPQUA Research Company

Layne Carter
NASA/Marshall Space Flight Center

Copyright © 2004 SAE International

ABSTRACT

Novel mesoporous bimetallic oxidation catalysts are described, which are currently under development for the deep oxidation (mineralization) of aqueous organic contaminants in wastewater produced on-board manned spacecraft, and lunar and planetary habitats. The goal of the ongoing development program is to produce catalysts capable of organic contaminant mineralization near ambient temperature. Such a development will significantly reduce Equivalent System Mass (ESM) for the ISS Water Processor Assembly (WPA), which must operate at 135°C to convert organic carbon to CO_2 and carboxylic acids. Improvements in catalyst performance were achieved due to the unique structural characteristics of mesoporous materials, which include a three-dimensional network of partially ordered interconnected mesopores (5-25 nm). This structure results in high surface area, high pore volume, and reduced distances for reactants and byproducts to diffuse to and from interior catalyst sites, as compared to the tortuous diffusion path in conventional, high surface area microporous (1-2 nm) supports. Mesocellular Foams (MCFs) composed of silica-zirconia solid solutions, chemically impregnated with platinum and ruthenium, were found to produce the most active catalyst. This catalyst proved capable of mineralization of acetic acid, a refractory organic, at ambient temperature.

INTRODUCTION

The recycling of wastewater to produce potable water is a core function of Environmental Control and Life Support Systems (ECLSS). Current plans for the International Space Station (ISS) call for recycling of humidity condensate and urine distillate, which are collected in a common storage reservoir.[1-4] The ISS Water Processor Assembly (WPA) designed for the U.S. Hab Module removes inorganic and organic contaminants using the series of processes shown schematically in Figure 1. [3,5]

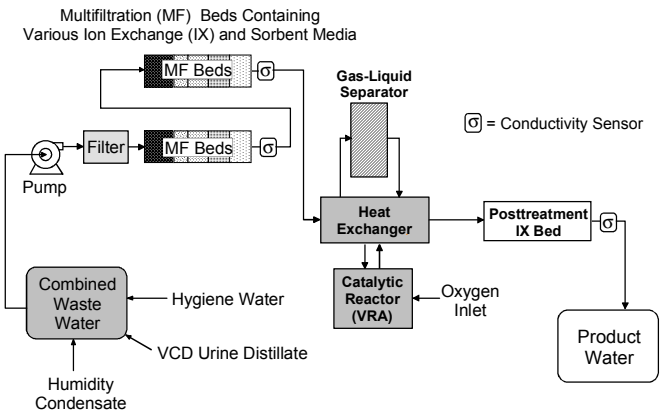

Figure 1. International Space Station Water Processor Assembly (WPA) Schematic.

Ionic contaminants are removed using ion exchange (IX), while the majority of organic contaminants are removed by adsorption onto activated carbon. These two processes are housed sequentially in the multifiltration (MF) subsystem. Highly polar, low molecular weight organic contaminants such as alcohols, acetone and other ketones, glycols, urea, aldehydes, some aromatic organics, and some ethers are not effectively removed by ion exchange or sorption. The elimination of these highly water soluble contaminants requires contaminant oxidation over a catalyst in the Volatile Removal Assembly (VRA)[6-8], a two-phase flow, packed bed, bubble reactor, that mineralizes many organics and also produces organic acids, which must be removed by a post-treatment IX bed. Significant operational and design complexity is associated with VRA operation. The VRA operates at 135°C (275°F) and is pressurized to 0.584 MPa (70 psig).[9,10] Other required equipment includes a pressurization pump, pressurized oxygen supply and delivery system, a two-stage heat

exchanger, and a gas-liquid separator (GLS) that removes unused oxygen and other gases upstream of the post-treatment IX beds. The GLS operates at 80°C to minimize dissolved gas in order to meet dissolved gas requirements for potable water.

The primary goal of this program was the development of ambient temperature catalysts with sufficient activity to replace the VRA catalyst. Such an achievement would reduce the ESM for the VRA in the U.S. Hab Module WPA, and for future ALS wastewater treatment systems aboard spacecraft, and on Lunar and planetary habitations that will require aqueous phase catalytic oxidation based post-treatment to meet water quality goals. When fully developed, ambient temperature catalysts can dramatically reduce the operating temperature and/or increase the degree of mineralization of organic contaminants in catalytic reactors. In the most straightforward case, replacement of the VRA with an ambient temperature reactor will reduce the WPA complexity by elimination of hardware required to process water at higher temperatures and pressures, and lower energy usage. Alternatively, the use of catalysts with higher activity than the conventional VRA catalyst at the current operation temperature will result in a smaller system with greater oxidation efficiency. Such catalysts will also be usable in future water reclamation systems that require posttreatment to meet potable water standards. This fundamental innovation can be applied to both physico-chemical and biological systems. Moreover, other situations can be conceived of, in which, these catalysts are employed to prevent the buildup of contaminants during water storage, or as an emergency backup system for potable water production aboard spacecraft.

The innovation employed to achieve high activity at ambient temperature was the use of novel, high surface area, mesoporous (i.e., 2 - 50 nm) materials as supports for conventional platinum and ruthenium noble metal catalysts. Mesoporous supports improve mass transfer of reactants and by-products between the bulk solution and catalytic sites. This is achieved by reduction of the tortuosity for diffusion of chemical species through the mesoporous support as compared to conventional microporous (i.e., < 2nm) supports.[11] Improved diffusion of reactants and by-products without reducing the number of catalytic sites is achieved through unique structural characteristics. Mesoporous supports are characterized by a partially ordered array of mesopores interconnected through mesoporous channels, porosity levels between 60 and 80%, and surface areas in excess of 500 m^2/g.

Conventional aqueous phase oxidation catalysts are composed of noble metals supported on Al_2O_3, ZrO_2, and activated carbon. For example, the VRA catalyst is a bimetallic noble metal catalyst supported on activated alumina. The VRA catalyst support, CPN, comes from a commercial source (i.e., Alcoa) and consists of amorphous, χ-, and γ- alumina phases. CPN is generally utilized as a gas or liquid phase sorbent for selected organic contaminants. The surface area and density of CPN are 320 m^2/g and 0.70 g/cm^3, respectively. This and similar catalysts have demonstrated reasonably high levels of aqueous phase oxidation activity for organic contaminants at temperatures between 100° and 130°C. The most active catalyst that has been developed for the oxidation of organic contaminants in water (RP-121) contains high levels of platinum and ruthenium (20 and 5 wt %) on a very high surface area (1800 m^2/g) activated carbon support.[6,7] Impregnation of the activated carbon with noble metals reduces the surface area by ~25% (1323 m^2/g).[12] Experimental data for RP-121 shows rapid oxidation of alcohols and moderate oxidation of glycols at ambient temperature.

In general, catalytic oxidation performance in the aqueous phase depends on multiple factors. The multistep oxidation mechanism requires diffusion of reactants to the catalytically active surface site, which may involve direct adsorption on the active site, or adsorption of the reactants onto the support followed by diffusion to the active site. Reactants must then combine at the catalyst site and oxidize. Reaction by-products must then desorb and diffuse away from the active site. Any of these steps may be rate limiting, and in general, catalytic activity is determined by five predominant factors: 1) surface reaction rate, 2) pore diffusion resistance, 3) film diffusion resistance, 4) intra-particle temperature gradients, and 5) film temperature gradients.[13-18]

For aqueous phase catalysts, oxidation rates depend primarily on factors 1 and 2. Factor 1 depends on catalyst composition, the number of catalyst sites, and the surface area, which in addition to increasing the available catalyst sites, also provides a surface for contaminant adsorption. Factor 2 depends primarily on the support structure. The excellent oxidation activity of RP-121 is due to catalyst site composition and the high surface area of the activated carbon support, which enables a very high noble metal loading and moderately strong contaminant adsorption. This combination results in excellent overall oxidation rates, even though turnover rate per site may be low. One limiting factor for RP-121 is mass transfer of contaminants and oxidation by-products to and from the majority of catalyst sites. Due to the structure of RP-121, the majority of surface area and catalyst sites are located within micropores that are buried deep within the support, which increases pore diffusion resistance.

Confirmation of this interpretation for RP-121 catalytic activity was achieved using nitrogen adsorption data at liquid nitrogen temperatures and the BJH model for adsorption isotherms.[19] These data were reduced to the pore size versus pore volume plot shown in Figure 2, which indicates that most of the pore volume and surface area comes from pores less than 2.0 nm in diameter.[12] Such small pores increase diffusion resistance by extending the average diffusion length through an

extended microchannel labyrinth. Consequently, many buried catalyst sites do not significantly participate in oxidation reactions.

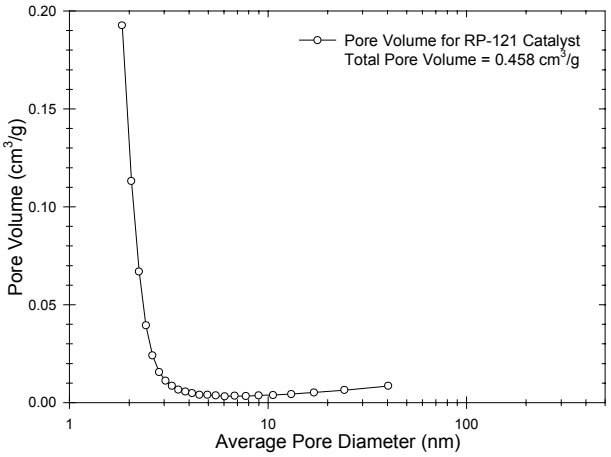

Figure 2. Pore Size Distribution for RP-121 Catalyst.

Minimizing the average diffusion length that reactants must travel to reach catalyst sites within the support and that byproducts such as CO_2 must travel to exit the support will decrease pore diffusion resistance. A new class of mesoporous materials, exhibiting precisely these physical characteristics, was expected to improve oxidation performance.[20-43] The bulk of the activity for the current program involved investigation of different mesoporous materials as aqueous phase oxidation catalyst supports.

Several approaches were investigated to improve the oxidation activity of catalysts based on mesoporous supports. These approaches involved modification of the support composition, structure, and surface properties. Four main groups of modified mesoporous supports were prepared. These included: 1) silica Mesocellular Foams (MCFs) with zirconia and alumina grafted onto the surface; 2) mesoporous alumina supports; 3) silica - zirconia solid solutions with a structure consisting of interconnected macropores whose surfaces were covered with mesopores (mixed porosity), and; 4) MCFs with a range of transition metal – silica compositions. The oxidation of acetic acid, a refractory organic contaminant, over catalysts based on these supports was then compared with a control catalyst designed to simulate the current VRA catalyst.

EXPERIMENTAL SECTION

SUPPORT PREPARATION

Two methods were used to prepare mesoporous silica supports, which contained transition and rare earth metal oxides such as niobium, aluminum, cerium, and zirconium oxide. In the first approach, mesoporous supports were fabricated using the properties of specific non-ionic surfactant – silica sol aqueous solutions to direct the growth of a silica network into a three dimensional structure with ordered mesopores. After calcination, other oxides were grafted onto the surface of the well-developed mesoporous silica. In the second method, a mixed aqueous sol with silica and other network forming species was gelled in the presence of structure directing surfactants, thereby producing mesoporous mixed oxides. Both methods resulted in homogeneous, monolithic gels. After thermal processing and size reduction, granular supports sized between 0.425 and 1.0 mm in diameter were produced. Platinum and ruthenium salts were then chemically adsorbed onto the support particles and thermally processed to produce supported catalysts.

Mesoporous alumina supports were fabricated in butanol solutions using a structure directing surfactant and aluminum oxide network forming precursors. Under these conditions, water was employed to initiate network formation. As with the silica-based mesoporous materials, platinum and ruthenium salts were then adsorbed onto the alumina particles and thermally processed to produce supported catalysts.

Mesocellular Foam (MCF) Silica Supports

Synthesis of silica MCFs was adapted from methods described in the literature, in which, particles and agglomerates were the primary products.[20-43] Material synthesis began with the dissolution of the structure directing surfactant in an aqueous HCl solution. The non-ionic surfactant of choice, EO_{20}-PO_{70}-EO_{20}, is an amphiphilic block copolymer, where EO = ethylene oxide and PO = propylene oxide. This polymer is comprised of a long poly(propylene oxide) (PPO) segment and two medium length poly(ethylene oxide) (PEO) segments with a molecular weight of 5800 daltons. In water, the copolymer blocks organize into micelles, in which, the hydrophobic PPO block preferentially locates at the core with the hydrophilic PEO block at the surface of the micelle. Next, a swelling agent, 1,3,5-trimethyl benzene (TMB), is added to the solution, which is sonicated to form a homogeneous, opalescent emulsion due to reorganization of hydrophilic and hydrophobic constituents. Then, tetraethyl orthosilicate (TEOS) is added to the stirred solution, which is heated to 40°C, resulting in gelation of the silica sol. Later, the temperature is raised to 75°C - 120°C, and the gel is allowed to age. During the aging cycle, self-assembly of individual micelles eventually forms a three-dimensional interconnected surfactant phase.[25-30]

In the acidic solution, the protonated hydrolyzed silica sol[25-28] condenses at the surface of the organized surfactant phase, forming a continuous silica network according to (1),

$$n\mathrm{Si(OCH_2CH_3)_4} + 2n\mathrm{H_2O} \rightarrow n\mathrm{SiO_2} + 4n\mathrm{CH_3CH_2OH} \quad (1).$$

During condensation, positively charged sol species preferentially associate with the hydrophilic EO outward-facing component of the organized surfactant phase.[25-30]

A continuous ever growing silica network begins to surround the interconnected surfactant phase. As this network expands outward, intergrowth between adjacent networks forms a three-dimensional silica gel structure. The presence of the swelling agent increases the size of the hydrophobic surfactant cores, which form templates for mesopore formation in the final MCF structure. At higher aging temperatures, the average hydrophobic core grows even larger due to changes in interfacial tension, and the structure matures.[29] In addition, the presence of ammonium fluoride, NH_4F, also enhances the maturation process through increased SiO_2 solubility. Numerous MCF preparations were evaluated.

After the formation of the 'green' monolithic gel, the samples are thoroughly washed and slowly dried. In normal drying of silica gels, the removal of water causes stress that leads to pore collapse and cracking.[38] Prevention of cracks in such bodies requires exchanging another solvent for water before drying or supercritical drying. The presence of a high level of surfactant in MCFs lowers capillary forces sufficiently to permit the removal of water without the formation of cracks. Consequently, slow drying removes water without stress, and the remaining surfactant and swelling agent can be removed in a controlled fashion. This is accomplished by slow heating of the monolithic gel to between 500° and 550°C. This thermal treatment removes organics and consolidates the MCF. An example of a calcined monolith is shown in Figure 3.

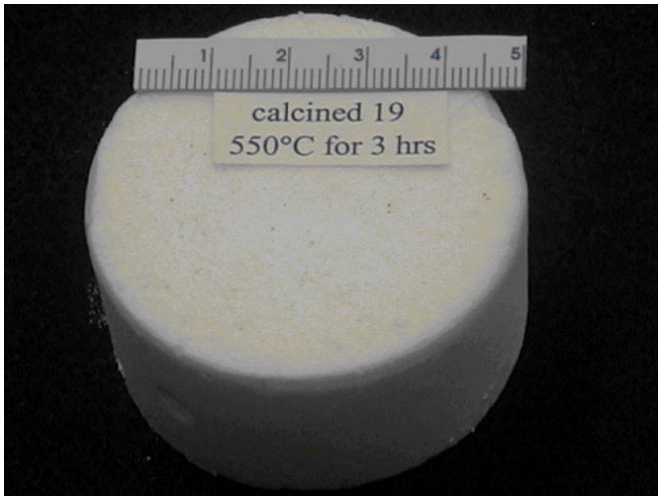

Figure 3. Calcined MCF Monolith (scale in cm).

Mesoporous Silica-Zirconia Supports

Several different SiO_2-ZrO_2 mesoporous materials were investigated. The SiO_2 - ZrO_2 mesoporous materials were synthesized according to the methods described by Takahashi *et al.*[39] and Wong *et al.*[40] Each approach yielded mesoporous materials with different structural characteristics.

In the first synthesis, the structure directing surfactant is polyethylene oxide, PO, with an average molecular weight of 100,000. PO is dissolved in an aqueous nitric acid solution. After a homogeneous mixture is achieved, the solution is cooled to 0°C. To this chilled solution, a mixture of zirconia and silica network forming species is added. The network formers include tetramethyl orthosilicate (TMOS), zirconium(IV) propoxide (ZP), and zirconium(IV) butoxide (ZB). This mixture is slowly added while maintaining the temperature between 0° and 5°C. To form more complex solid solutions, cerium chloride hydrate ($CeCl_3 \bullet 7H_2O$) and aluminum chlorohydrate ($(Al_{13}O_4(OH)_{24}(H_2O)_{12})Cl_7$) were included in the original PO solution. Initially, a cloudy solution forms; however, the solution clears upon stirring, forming a mixed sol. Aging this sol at 40°C results in the formation of a clear gel. The gel densifies with time into a mixed silica - zirconia network that continues to shrink and eventually a cracked translucent monolith is formed. The monolith is then extensively washed with deionized water to remove the PEO surfactant. Drying the rinsed monolith between 40° and 100°C, causes additional cracking. After drying, the gel pieces are slowly heated to 550°C in air. A network of macropores with mesoporous walls characterizes the structure of this material. This structure results in higher density and greater crystallinity than mesoporous silica, while retaining similar surface areas. Formation of this structure is driven by phase separation of solvent, PEO, and hydrolyzed SiO_2 - ZrO_2 rich phases.

The second SiO_2-ZrO_2 material preparation utilized the same surfactant (i.e., EO_{20}-PO_{70}-EO_{20}) employed for the silica MCF preparation. A slightly less acidic aqueous solution containing this amphiphilic surfactant is used in this preparation. First, zirconyl chloride, ($ZrOCl_2$), is introduced, forming a clear solution. Then, TMB is added to this mixture followed by ultrasonication to form an emulsion. TEOS is stirred into the mixture and ultrasonicated. This solution is aged at 40°C for 20 hours during which a translucent monolithic gel forms. This is followed by another 20 hours at 75°C to mature the gel. These gels are then rinsed and dried, resulting in a highly fractured monolithic structure which is fired at 550°C.

Mesoporous Alumina Supports

The synthesis of alumina (i.e., Al_2O_3) mesoporous materials was adapted from the preparation scheme of Zhang *et al.*[41] First, butanol, EO_{20}-PO_{70}-EO_{20}, and aluminum tri-sec-butoxide ($Al(OC(CH_3)_3)_3$) are mixed together until a clear solution is formed. This solution is then rapidly hydrolyzed by the addition of water, creating a viscous opalescent gel. Aging this gel at 40°C for 20 hours forms a clear gel. Additional aging at 75°C for 6 hours and 100°C for 20 hours further consolidates the gel. Solvent is then drained from the sample, which is dried at 100°C resulting in a cracked gel. These pieces are then fired at 550°C.

Aluminum Oxide and Zirconium Oxide Grafted MCF.

Al_2O_3 and ZrO_2 were also grafted onto the surface of previously prepared silica MCFs. The preliminary method was an adaptation of the procedure previously used by Mokaya *et al.*[42,43] to graft Al_2O_3 onto MCM-41 mesoporous silica. The Al source is aluminum chlorohydrate, $(Al_{13}O_4(OH)_{24}(H_2O)_{12})Cl_7$, a complex polycation prepared by acidification of an $Al(OH)_3$ solution to pH 3.5 with HCl. The Zr source is zirconium oxychloride, $ZrOCl_2$. A monolithic MCF is crushed and sieved to produce particles between 0.425 and 1.00 mm. These particles are immersed in 50 mL of water containing the appropriate quantities of aluminum chlorohydrate and zirconium oxychloride salts. The beakers are placed in a vacuum desiccator, which is evacuated to remove air and thoroughly wet the particle surfaces. These samples are dried at 40°C for 48 hours followed by 24 hours at 75°C and 6 hours at 100°C. The absence of salt deposits indicates that drying is homogeneous. These samples are fired at 650°C.

CATALYST PREPARATION

Platinum and ruthenium impregnated catalysts were prepared using a variety of SiO_2 - ZrO_2 mesoporous materials (including other transition metals and rare earth oxides), an Al_2O_3 mesoporous material, Al_2O_3 grafted onto two different MCFs, and ZrO_2 grafted to two different MCFs. The approach used to impregnate platinum and ruthenium on the support utilized adsorption of aqueous ionic species of these two metals on the mesoporous support surface. Proper selection of solution chemistry, catalyst solution species, and pH is required to achieve homogeneous impregnation. The impregnated support is dried at 100°C for several hours. After drying, the support is fired under a reducing gas mixture containing H_2, N_2, and H_2O at 550°C for 120 to 180 minutes.

A simulated VRA catalyst was prepared to serve as a control for comparison of results from the mesoporous catalysts. This catalyst utilized the same support as the actual VRA catalyst. Platinum and ruthenium were applied to this support using the same techniques that were used for the mesoporous catalysts.

CATALYST TESTING

Catalysts were evaluated in the test stand shown in Figure 4. In this configuration, a catalyst filled plug flow reactor is fed an oxygen saturated acetic acid solution. A pressure regulator controls the reactor pressure independently so that during higher temperature operation oxygen will remain dissolved within the reactor. Under controlled flow conditions, the effluent concentration of acetic acid is determined as a function of flow rate. The oxidation data are then reported as fractional conversion as a function of contact time (reactor space-time).

Global oxidation rates were evaluated using a pseudo first order plug flow kinetic model. This model provides a practical approach for gathering and comparing catalytic oxidation data without detailed knowledge of the reaction mechanism, although an implicit assumption of this model is that access to catalyst sites is linearly dependent on concentration. This model has previously been used with great success in characterizing catalyst performance for the aqueous phase oxidation of organic contaminants at moderate temperatures between 100° and 130°C.[44-47]

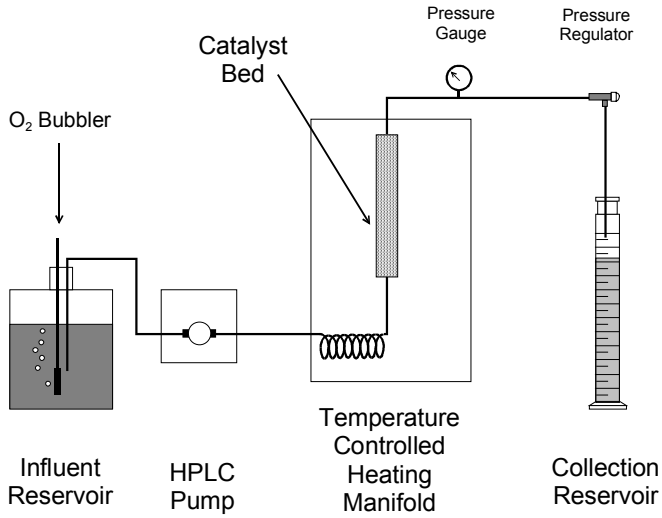

Figure 4. Catalyst Evaluation Test Stand.

In oxidation reactions involving dissolved oxygen and an organic contaminant, the presence of a large oxygen excess eliminates the O_2(aq) concentration term from the rate expression given by,

$$\frac{dC}{dt} = k\, C_{O_2} C_A \qquad (2).$$

The constant O_2(aq) concentration term is incorporated into the rate constant and following integration the pseudo first order dependency shown in (3) results,

$$C = C_o e^{-k_{pseudo} t} \qquad (3),$$

where C is the outlet concentration, C_o is the inlet concentration, k_{pseudo} is the pseudo first order reaction rate constant in s^{-1}, and t is the residence time within the reactor (i.e., reactor space-time). The value of t depends on the void volume, V_r,, within the catalyst bed, and the flow rate, Q. The reactor space-time, t, is determined according to (4),

$$t = \frac{V_r \phi}{Q} \qquad (4),$$

where ϕ is the fractional void volume of the packed catalyst bed and V_r is the reactor volume. When the fractional void volume is not known, the empty bed volume is used in place of the fractional void volume and ϕ becomes 1. Plug flow conditions were validated based on flow rates, reactor length, and catalyst particle size. Pseudo first order rate constants (k_{pseudo}) for the first order plug flow rate law were derived from the resulting (C, t) ordered pairs using the Levenberg-Marquardt

method.[48] Correlation coefficients (r^2) for the derived rate constants were calculated using a linear regression of experimentally observed concentrations versus those calculated from (3).

The temperature dependence for the rate constants determined in (3) were fitted to the Arrhenius expression given by (5),

$$k(T) = Ae^{-\frac{E_a}{RT}} \quad (5),$$

as (1/T, ln k_{pseudo}) ordered pairs using a least squares approximation to a linear equation. Activation energy (E_a), and frequency factor (A) were determined from the slope and intercept, respectively. The Arrhenius expression assumes that the reaction mechanism remains unchanged over the applicable temperature range. When this condition is met, the E_a and A values can be used to predict oxidation rates at other temperatures.

A comparison of k_{pseudo} and E_a data for different catalysts was used to select the best catalyst for use in a specific temperature range. A potential problem with this general approach will occur if the reaction mechanism changes over the temperature range, or if adsorption phenomena are sufficiently significant that Langmuir-Hinshelwood rate expressions are more appropriate.

EXPERIMENTAL RESULTS

PHYSICAL CHARACTERISTICS OF MESOPOROUS CATALYST SUPPORTS

Mesoporous support surface areas were determined using the BET model for the multilayer adsorption of nitrogen on surfaces at liquid nitrogen temperature.[49] Pore size distributions were determined using the BJH method, which models the adsorption and capillary condensation over a range of pressures.[19] In the BJH model, pores are filled stepwise as the pressure is raised in accordance with a modified Kelvin equation that relates the relative pressure required to condense gas within pores of different radii.[50] An important aspect of the type IV isotherms common to mesoporous supports is the existence of hysteresis between adsorption and desorption isotherm branches. Small-angle X-ray scattering (SAXS) and TEM studies of mesoporous materials have shown that the average pore size correlates well with that determined from the adsorption isotherm, while the size of channels that connect pores correlates well with that calculated from the desorption isotherm.[25]

Mesocellular Foam Catalyst Support

Adsorption - desorption isotherms were determined for the silica mesocellular foam designated as MCF 24. These type IV isotherms, with pronounced hysteresis at high relative pressures, are shown in Figure 5.[50] The surface area for this MCF was 491 m^2/g and the total pore volume per gram was 1.63 cm^3/g. Based on the density for silica (2.64 g/cm^3), MCF 24 contains 81.1% open porosity. These data demonstrate the effectiveness of this approach for the synthesis of monolithic MCFs with high porosity and surface area.

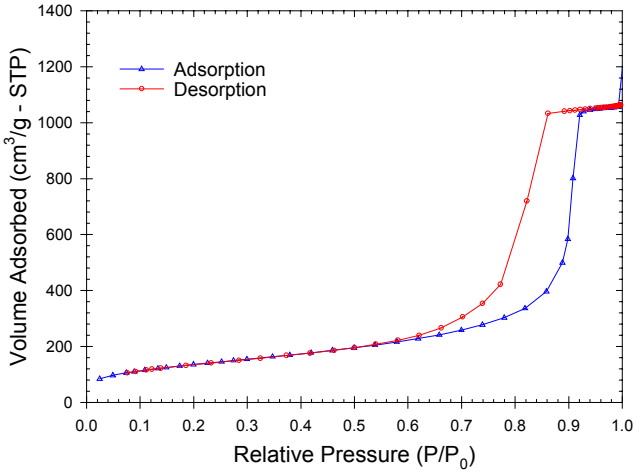

Figure 5. MCF Adsorption and Desorption Isotherms.

The BJH pore volume versus pore size distributions for adsorption and desorption isotherms are shown in Figure 6. The pressure dependencies for adsorption and desorption isotherm branches respond to two factors, the pore size radius and exterior access to pores of that radius.[50] During adsorption, condensation occurs throughout the three-dimensional array of pores and connecting channels. During desorption, the situation changes because evaporation of condensed nitrogen initially occurs from smaller radius channels. According to the Kelvin expression, this shifts equilibrium to a lower pressure. Based on the adsorption isotherm branch the mesopore size in MCF 24 is approximately 22 nm in diameter, while the desorption branch indicates that somewhat smaller channels of approximately 11 nm in diameter separate the large mesopores. These data illustrate the bimodal pore size distribution characteristic of MCFs.

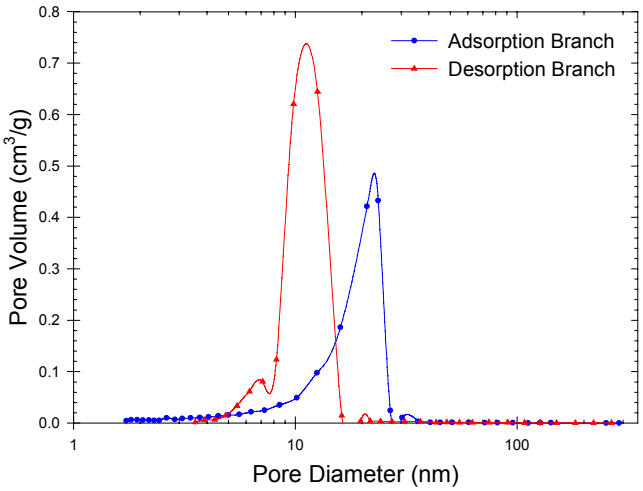

Figure 6. MCF Pore Sizes.

Mesoporous Silica-Zirconia Catalyst Support

The fabrication of a mesoporous silica - zirconia solid solution was an important goal, since the activity of aqueous phase oxidation catalysts also depends on the support composition. Strongly acid zirconia sites on the support influence catalytic reactions and contaminant adsorption. The adsorption/desorption isotherms for the 66.2 wt% silica and 33.8 wt% zirconia mesoporous support, 1C, are shown in Figure 7. This type IV isotherm exhibits hysteresis between relative pressures of 0.6 and 1.0. The surface area for 1C is 476 m^2/g, which is similar to that for MCF 24. The total pore volume per gram for 1C is 0.734 cm^3/g. Using a density of 3.23 g/cm^3 for the solid solution (i.e., a linear combination of 2.64 g/cm^3 for silica and 5.6 g/cm^3 for zirconia), 1C contains 70.4% open porosity. Pore volume distributions for adsorption and desorption branches of the isotherms are shown in Figure 8. The bimodal pore size distribution indicates mesopores 9.7 nm in diameter separated by channels 6.2 nm in diameter. Although the pore size of 1C is somewhat smaller than that of silica MCFs, the structural properties meet the objectives for mesoporous catalysts.

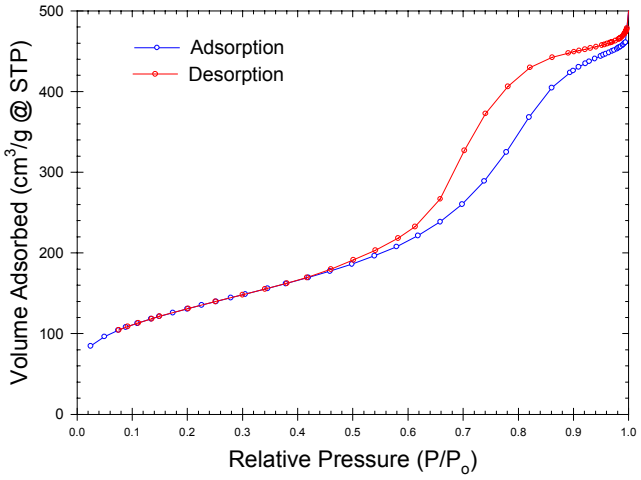

Figure 7. Adsorption/Desorption Isotherms for 1C.

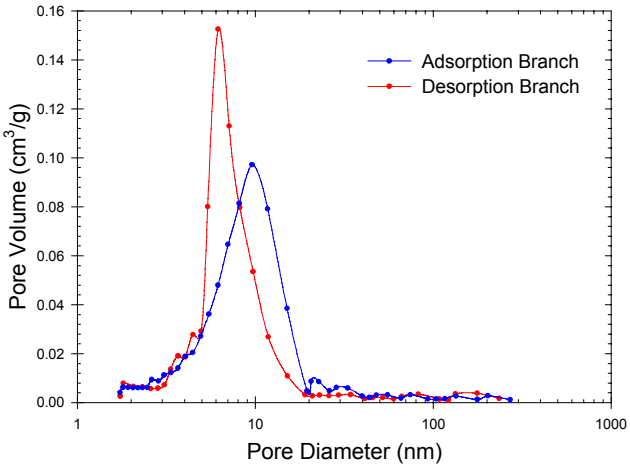

Figure 8. Pore Size Distributions for 1C.

Macroporous/Mesoporous Silica-Zirconia Catalyst Support

The second silica - zirconia support contained 90.15 wt % SiO_2 and 9.85 wt % ZrO_2. According to the literature,[39] this material contains both macropores and mesopores. The adsorption/desorption isotherms for this support, 6A, are shown in Figure 9. This type I isotherm exhibits little hysteresis[50], which indicates a uniform pore structure. The surface area for 6A is 496 m^2/g with a total pore volume per gram of 0.256 cm^3/g. The density was estimated to be 2.94 g/cm^3 based on a linear combination of silica and zirconia densities. Based upon this assumption, 6A contained 42.9 % open porosity. The lower porosity as compared to 1C was reflected in the greater mechanical strength of this material. Pore volume distributions are shown in Figure 10, which indicated that the majority of mesopores are between 2 to 3 nm. Using the BJH data, the cumulative surface area of pores between 1.7 and 300.0 nm is 186 m^2/g or 37.5 % of the BET surface area. Based on these data, the structure of 6A is consistent with mixed porosity containing both micropores and mesopores.

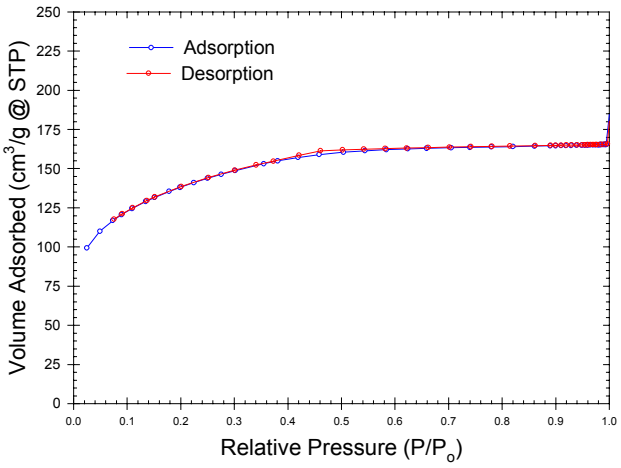

Figure 9. Adsorption/Desorption Isotherms for 6A.

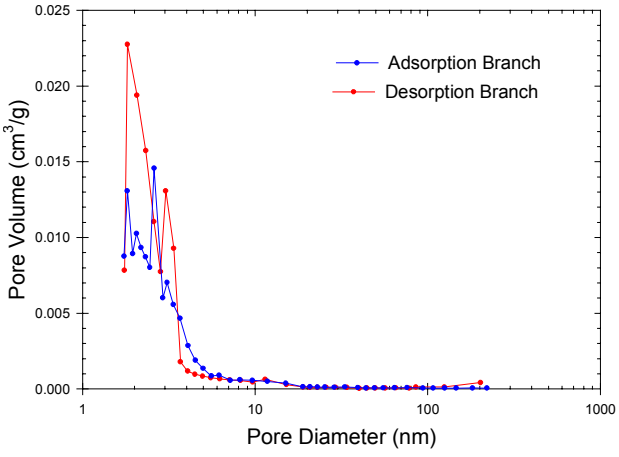

Figure 10. Pore Size Distributions for 6A.

Mesoporous Alumina Catalyst Support

Adsorption and desorption isotherms for the alumina mesoporous support, 3B, are shown in Figure 11. The type IV isotherms exhibit significant hysteresis as expected for interconnected mesoporosity. The surface area for 3B is 369 m^2/g. The pore volume is 1.369 cm^3/g, which based upon an alumina density of 3.7 g/cm^3, gives an open porosity of 83.5%, the highest among the mesoporous materials that were evaluated. The pore sizes calculated from adsorption and desorption isotherms are shown in Figure 12, which indicate a multimode pore size distribution. Two pore sizes, 12 and 28 nm, were derived from the adsorption branch, while an average pore size of 10 nm was derived from the desorption branch. The structure of 3B is consistent with the presence of variable sized mesopores interconnected with a mesoporous window.

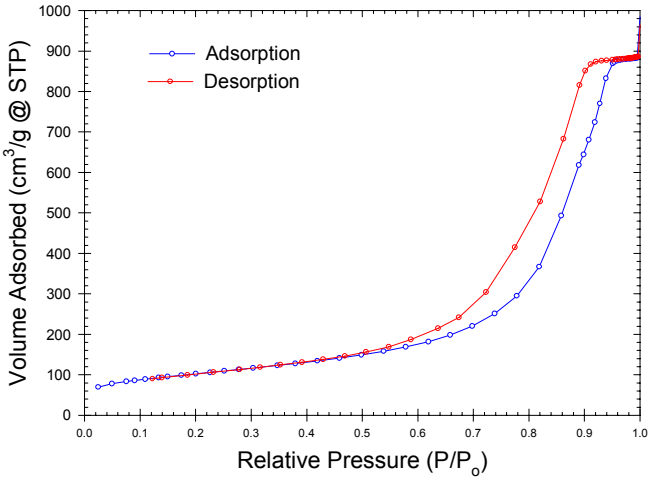

Figure 11. Adsorption and Desorption Isotherms for Alumina 3B.

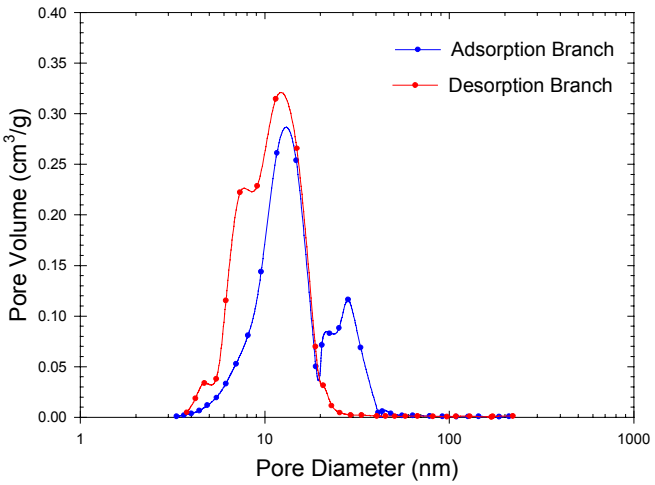

Figure 12 Pore Sizes from 3B Adsorption/Desorption Isotherms.

CATALYTIC OXIDATION RESULTS

Acetic acid was oxidized over the control CPN based catalyst and numerous mesoporous catalysts at temperatures between 20° and 73°C. The challenge solution typically contained 10 mg/L (0.1665 mM) of acetic acid equilibrated with oxygen at atmospheric pressure (i.e., 101.4 kPa or 14.7 psi) at 20°C. This translates into 43 mg/L of dissolved oxygen, a four-fold excess of that required for complete oxidation. Under these conditions, pseudo first order reaction kinetics are applicable.

The kinetic evaluation of acetic acid oxidation was performed on selected catalysts. These included: 1) the control CPN based platinum and ruthenium catalyst, 2) platinum and ruthenium catalysts supported on silica MCF with Al_2O_3 grafted onto the surface; 3) platinum and ruthenium catalysts supported on mesoporous Al_2O_3; 4) platinum and ruthenium catalysts supported on SiO_2 - ZrO_2, SiO_2 - ZrO_2 - CeO_2, and SiO_2 - ZrO_2 - Nb_2O_5 solid solutions characterized by interconnected macropores whose surfaces were covered with mesopores (i.e., mixed porosity), 5) ruthenium catalysts supported on SiO_2 - ZrO_2 - CeO_2, and; 6) platinum and ruthenium catalysts supported on SiO_2 - ZrO_2 MCFs. Of these, the most significant information was obtained from the control catalyst, the platinum and ruthenium catalyst supported on SiO_2 - ZrO_2 - CeO_2, and platinum and ruthenium catalysts supported on the SiO_2 - ZrO_2 MCF.

Control Catalyst

Initial catalyst tests using the CPN based control catalyst indicated that the Al_2O_3 support strongly adsorbed acetate. A breakthrough curve for the control catalyst when challenged with 10 mg/L of acetic indicated an acetic acid sorption capacity of 0.049 mEq/g. This presented difficulties for the characterization of oxidation kinetics, since the kinetics evaluation procedure assumes that the difference between inlet and outlet concentrations depends only on the extent of oxidation reactions, which occur during passage through the reactor. Adsorption or desorption of acetate invalidates the determination of acetate oxidation by this method. The affinity of acetate for the Al_2O_3 surface is related to the surface charge of the CPN support. Figure 13 shows the surface charge for CPN particles as a function of pH. These data indicate that the isoelectric point for the CPN support is 7.22. Below this pH, the surface is positively charged due to protonated surface sites, while above this pH, the surface is progressively more negatively charged until all surface sites become deprotonated. At the isoelectric point, the surface is uncharged. The surface charge strongly influences adsorption of the acetate anion from solution. The surface charge for Al_2O_3 at slightly acidic pHs is positive, so, CPN will adsorb acetate anions from a 10 mg/L acetic acid challenge solution since its pH in pure water will be 4.34. Acetate adsorption/desorption was also evident for mesoporous Al_2O_3 supports and for supports consisting of Al_2O_3 grafted onto the MCF support surface.

The method utilized to acquire valid acetate oxidation data involved establishing adsorption equilibrium prior to

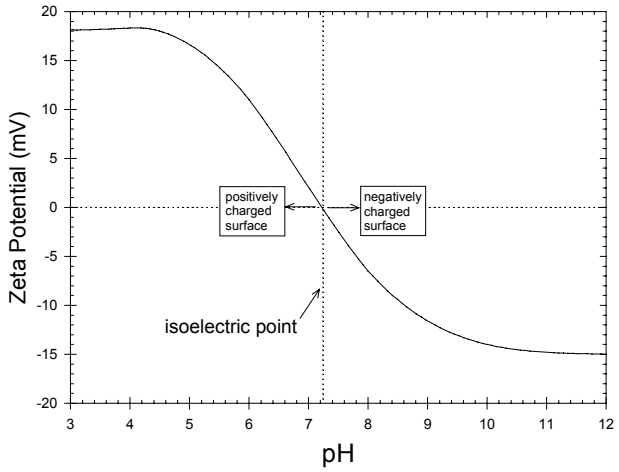

Figure 13. Zeta Potential for CPN Al_2O_3 Catalyst Support.

oxidation experiments. This was accomplished by flowing an anoxic acetic acid solution through the reactor until influent and effluent acetic acid concentrations were equalized. Once adsorption/desorption equilibrium was established, the influent was saturated with dissolved oxygen and oxidation data were collected as a function of contact time. Contact times were varied between 110 and 625 seconds. The results are shown in Figure 14. The k_{pseudo} is extremely low, 2.79 x 10^{-5} s^{-1} with significant data scatter caused by minor temperature variations resulting in adsorption/desorption of acetate anions.

The temperature was raised to 38°C, and the effluent to influent acetic acid ratio was monitored. After 400 mL of throughput, results showed that the effluent concentration was 125% of the influent. These data clearly indicated that the increase in temperature caused desorption of acetic acid from the control catalyst. After

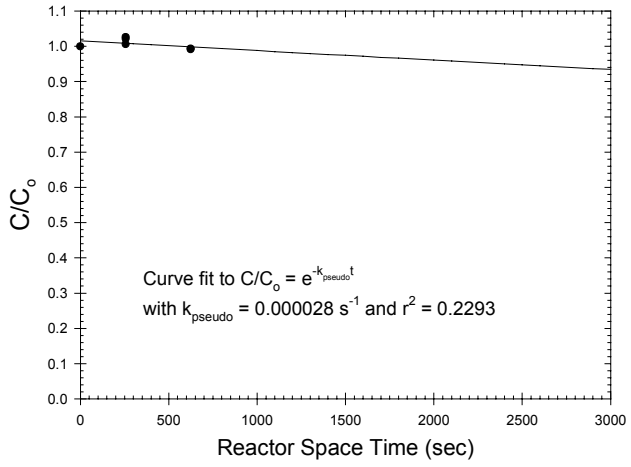

Figure 14. Acetic Acid Oxidation in 2.5 cm^3 Bed of CPN Catalyst (1.70g) at 20°C.

600 mL of throughput, the effluent level declined to the influent level. At this point, oxidation tests at 38°C were initiated. The contact time was varied between 116 and 625 seconds. The pseudo first order kinetics fit to the data is shown in Figure 15. The k_{pseudo} is 3.04 x 10^{-4} s^{-1}, ten times greater than the value at 20°C.

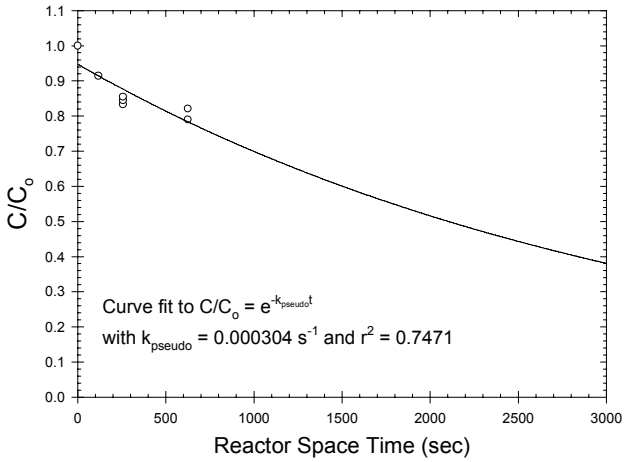

Figure 15. Acetic Acid Oxidation Over CPN Catalyst at 38°C.

The temperature was then raised to 63°C and in a similar manner to the lower temperature run, acetate desorption was evident for nearly 500 mL of throughput. When the temperature was raised to 63°C, kinetic data resulted in a k_{pseudo} of 6.88 x 10^{-5} s^{-1}, which is lower than the value determined at 38°C.

These data indicate that raising the temperature eventually results in a change in the oxidation mechanism. If one assumes a reaction mechanism involving adsorbed acetate and dissolved oxygen (i.e., Rideal Mechanism), then four rate-controlling steps are possible. These include: 1) the rates of diffusion of acetate and oxygen through the bulk solution to the catalyst surface; 2) the rate of acetate adsorption onto the catalyst surface; 3) the intrinsic chemical reaction rate at the catalyst surface, and; 4) the rate of desorption of reaction by-products. Rates for steps 1, 3, and 4 increase with temperature to varying degrees (step three increases exponentially as per the Arrhenius relation). In contrast, adsorption rates diminish sharply with temperature, and consequently, the temperature dependence for the oxidation rate may respond in a complex manner.

At lower temperatures, strong adsorption of acetate is favored and acetate and oxygen are in plentiful supply at the catalyst sites. The oxidation rate is limited only by the intrinsic rate of chemical reaction. However, as temperature is raised, less acetate is adsorbed on the catalyst surface. In this case, the acetate is not in plentiful supply on the catalyst surface and only a fraction of the catalytic sites are active at any given time. The overall oxidation rate is limited by the rate of adsorption of acetate from solution. The global reaction rates may

rise more slowly with temperature than expected for a simple thermally activated process, or even eventually decline. Under these circumstances, the use of Langmuir-Hinshelwood rate laws would be more appropriate. Regardless, the reaction rates for acetic acid over the simulated VRA catalyst were very low at temperatures between 20° and 63°C.

Mesoporous Alumina Supported Catalyst Results

The pseudo first order oxidation rate constants for platinum and ruthenium catalysts supported on mesoporous Al_2O_3 (3B) and on an Al_2O_3 grafted MCF (23_Al_1) are higher than that for the control catalyst. The k_{pseudo}'s are from 1.5 to 14 times higher than the control catalyst in the temperature range from 22° to 60°C, indicating improvement in oxidation efficiency. These improvements originate from the structural properties of these two supports since the compositions were similar to the control catalyst. Specifically, the surface area, pore size, and total porosity were 369 m^2/g, 10 to 28 nm, and 83.5 % for 3B; and 491 m^2/g, 10 to 21 nm, and 81.1% for 23_Al_1. As with the control catalyst, the temperature dependence indicates that the oxidation mechanism changes with temperature.

Macroporous - Mesoporous Mixed Oxide Catalyst Results

A series of catalysts was evaluated that utilized supports prepared using the method of Takahashi, et al,[39] which results in a mixed macroporous - mesoporous structure that is mechanically more robust than other mesoporous supports. The supports included 6A (90.15 wt% SiO_2 and 9.85 wt % ZrO_2), 8A (90.0 wt % SiO_2, 7.5 wt% ZrO_2, and 2.5 wt% CeO_2), and 9A (90.0 wt% SiO_2, 5.0 wt% ZrO_2, and 5.0 wt% Nb_2O_5), which provided a range of acid site forming transition metal oxides and a rare earth oxide. These supports were expected to be similar to 6A in surface area, pore size, and total porosity. Of these catalysts, 8A gave the highest pseudo first order rate constants.

A 2.5 cm^3 reactor containing 0.60 g of 8A catalyst particles between 0.425 and 1.00 mm in diameter was fed the standard challenge solution. Relative acetic acid oxidation versus reactor space-time at 22°C is shown in Figure 16. The k_{pseudo} is 5.81 x 10^{-4} s^{-1} with an r^2 of 0.9873, approximately twenty times that of the control catalyst. The oxidation of acetic acid at 46°C is shown in Figure 17.

These two data points were fitted to the Arrhenius expression. The slope of this curve yielded an Arrhenius activation energy, E_A, of 5.0 kcal/mole. Using this expression, the approximate contact time required to achieve 99% oxidation at 95°C is 1902 seconds, while at 75°C approximately 2818 seconds are required.

Mesoporous Silica - Zirconia Supported Catalyst Results

The oxidation performance of platinum and ruthenium catalyst supported on mesoporous silica - zirconia 1C

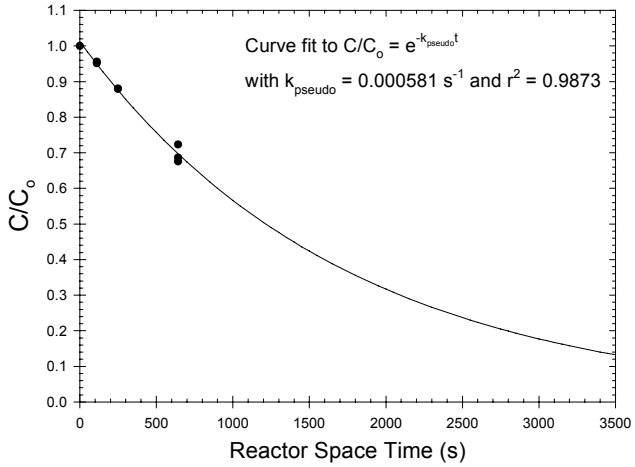

Figure 16. Acetic Acid Oxidation Over 8A at 22°C.

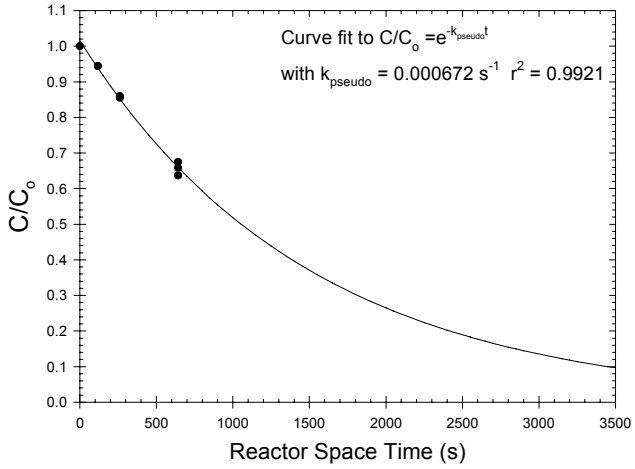

Figure 17. Acetic Acid Oxidation Over 8A at 46°C.

was evaluated using the standard challenge solution. A 2 cm^3 reactor was filled with 1.42 g of this catalyst consisting of 0.425 to 1.00 mm particles. Contact times were varied between 45 and 493 seconds at 21°C. The ratio of effluent over influent acetate concentration is plotted in Figure 18 as a function of contact time (i.e., reactor space-time). The k_{pseudo} is 1.38 x 10^{-3} s^{-1} with an r^2 of 0.9763. At the longest contact time, approximately 51% of the acetic acid is oxidized. This k_{pseudo} is nearly 50 times that of the control catalyst and the highest obtained for all of the mesoporous supports that were tested. These data clearly demonstrate dramatic improvements in oxidation activity for catalysts based on mesoporous supports.

The temperature was raised to 34°C and the experiment repeated. These results are shown in Figure 19. At the slowest flow rate, nearly 72% of the acetic acid was oxidized. The k_{pseudo} at 34°C is 2.31 x 10^{-3} s^{-1}, nearly double that obtained at 21°C. The oxidation results for

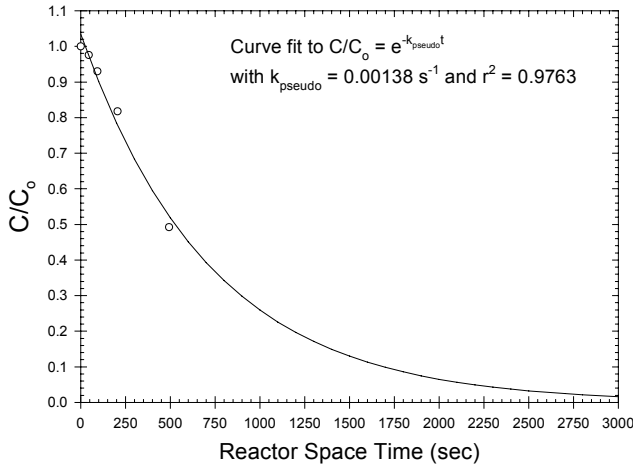

Figure 18. Acetic Acid Oxidation Over 1C at 23°C.

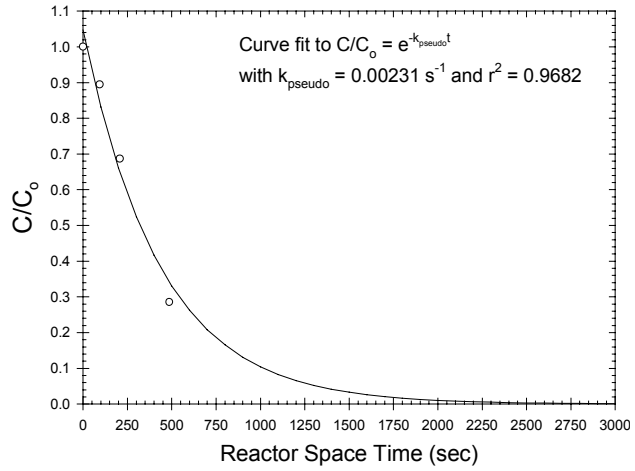

Figure 19. Acetic Acid Oxidation Over 1C: at 34°C.

this catalyst near ambient temperature clearly demonstrates the capability to oxidize acetic acid at low temperature. Performance of 1C was superior to other mesoporous catalysts.

These two data points were fitted to the Arrhenius expression. The slope of this curve yielded an Arrhenius activation energy of 7.1 kcal/mole. Projecting the oxidation rate to higher temperatures showed that the approximate contact time required to achieve 99% oxidation for this catalyst at 95°C is 287 seconds and at 75°C is 512 seconds.

The pseudo first order rate constants for the various catalysts are shown in Table 1. The superior performance of the 1C catalyst is clearly evident. Consequently, long-term tests were undertaken to determine oxidation stability. The long-term performance for this catalyst is shown in Figure 20. These data show stable acetic acid oxidation for over 3000 bed volumes without an indication of catalyst degradation.

Utilization of the platinum and ruthenium catalyst supported on 1C has demonstrated a nearly fifty-fold

Table 1. Rate Constants for Tested Catalysts.

Catalyst	k_{pseudo} (s^{-1})	Temperature (°C)
CPN	2.80×10^{-5}	20
CPN	3.04×10^{-4}	38
8A	5.81×10^{-4}	22
8A	6.72×10^{-4}	46
1C	1.38×10^{-3}	23
1C	2.31×10^{-3}	34

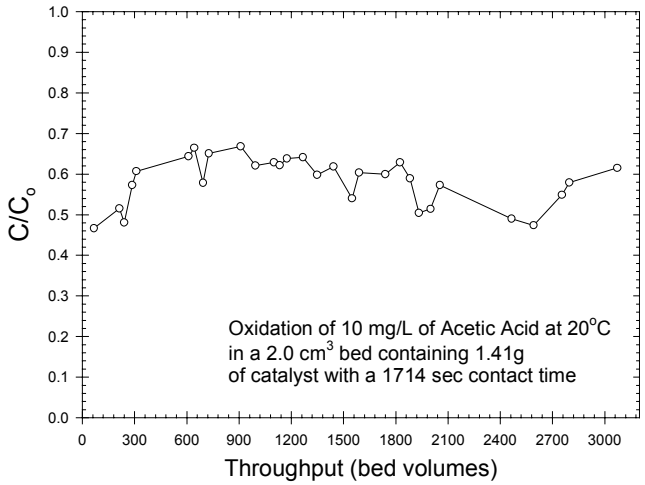

Figure 20. Stability for Long-Term Acetic Acid Oxidation Over Mesoporous Catalyst 1C.

increase in oxidation activity for a refractory organic contaminant, acetic acid. These results indicate that use of mesoporous materials as supports for noble metal catalysts can dramatically improve oxidation performance and realize ambient temperature oxidation of organic contaminants in water. Continued development of this line of research offers the potential to process contaminated water at much lower temperatures and pressures, which will result in lower ESMs for processes required to treat a wide variety of wastewaters in space-based applications. Utilization of advanced catalysts such as these will improve water treatment systems in general and offer engineers greater flexibility in meeting ECLSS and ALS performance goals.

CONCLUSIONS

The development of catalysts capable of oxidizing acetic acid, a refractory organic contaminant, at ambient temperature was successfully achieved during this Phase I project. When fully developed, ambient temperature catalysts can be employed in the VRA or similar reactors to increase the degree of mineralization of organic contaminants and to dramatically reduce operating temperature. This will lower complexity of the Water Processor Assembly (WPA) by elimination of hardware required to process water at higher temperatures and pressures. Alternatively, the use of catalysts with higher activity than that of the conventional

VRA catalyst at the current operating temperature will result in smaller system size and/or greater oxidation efficiency. Such catalysts will also be beneficial in future water reclamation systems that require posttreatment to meet potable water standards. This fundamental innovation can be applied to both physico-chemical and biological systems. Moreover, other situations can be conceived of, in which, such catalysts can be employed to prevent the buildup of contaminants during water storage, or may be used as an emergency backup system for the potable water production.

The core innovation used to produce ambient temperature noble metal catalysts was the development of catalyst supports with reduced mass transfer resistance. Methods were developed for the preparation of supports that exhibit substantial improvements with respect to properties that have been identified as the primary factors limiting the performance of the most active aqueous phase oxidation catalysts known to date. These properties include interconnected mesoporosity (5-25 nm), high porosity (60-80%), and high surface area (300-500 m^2/g). These structural features minimize pore diffusion resistance by reducing the diffusion length through the porous labyrinth in the support that is required to reach catalyst sites. This was accomplished without sacrificing surface area. These supports provide superior oxidation activity through substantially improved exchange of reactants and reaction by-products between catalyst sites and the bulk solution, as compared to conventional supports. The preparation of these innovative supports utilized the structure directing properties of surfactants. These surfactants direct the self-assembly of a three-dimensional network of partially ordered channels and pores built within an amorphous oxide network. Supports were prepared from silica, transition metal grafted silica, alumina, and silica – transition metal oxide solid solutions. Mesocellular foams (MCFs) composed of silica-zirconia solid solutions, which were chemically impregnated with platinum and ruthenium, produced the best catalysts.

The best MCF catalyst was compared with a simulated VRA catalyst for the oxidation of a refractory organic, acetic acid, at ambient temperature. The MCF catalyst's physical properties included a surface area of 476 m^2/g, 70.4% open porosity, and 9.7 nm mesopores connected by 6.2 nm channels. The simulated VRA catalyst was composed of platinum and ruthenium on the same support utilized in the current VRA catalyst. The noble metal levels on both catalysts were identical. The pseudo first order oxidation rate constant for the MCF catalyst was nearly 50 times higher than that of the simulated VRA catalyst at ambient temperature. These exciting results document the success of this innovative approach to improved catalyst performance. The full development of this catalyst technology during a Phase II program will augment current water recovery methods and lead to enhanced capabilities which may be incorporated into future water recovery systems.

ACKNOWLEDGMENTS

This work was supported by the National Aeronautics and Space Administration's Marshal Space FIght Center, Huntsville, Alabama, under contract NAS8-03019.

REFERENCES

1. Carter, D.L.; D.W. Holder, K. Alexandre, R.G. Shaw; and J.K. Hayase, Preliminary ECLSS Waste Water Model. SAE Technical Paper Series 951150, presented at the 21st International Conference on Environmental Systems, San Francisco, 1991.
2. Carter, D.L.; H. Cole, M. Habercom, G. Griffith, and L. Slivon, Determination of Organic Carbon and Ionic Accountability of Various Waste and Product Water Derived from ECLSS Water Recovery Tests and Spacelab Humidity Condensate. SAE Technical Paper Series 921313, presented at the 22nd International Conference on Environmental Systems, Seattle, 1992.
3. Carter, D.L.; and R.M. Bagdigian, Phase III Integrated Water Recovery Testing at MSFC: Single Loop Test Results and Lessons Learned. SAE Technical Paper Series 932048, presented at the 22nd International Conference on Environmental Systems, Colorado Springs, 1993.
4. Sauer, R.L.; L.M. Pierre, J.R. Schultz, Y.E. Sinyak, V.M. Skuratov, N.N. Protasov, and L.S. Bobe, Chemical Analysis of Potable Water and Humidity Condensate: Phase One Final Results and Lessons Learned. SAE Technical Paper Series 1999-01-2028, presented at the 29th International Conference on Environmental Systems, Denver, 1999.
5. Bagdigian, R.; D.S. Parker, and E.W. O'Connor, ISS Water Reclamation System Design. SAE Technical Paper Series 1999-01-1950, presented at the 29th International Conference on Environmental Systems, Denver, 1999.
6. Akse, J.R. and C.D. Jolly, Catalytic Oxidation for Treatment of ECLSS and PMMS Waste Streams, *Regenerative Life Support Systems and Processes*, Behren, A., MacElroy, R.D., and Reysa, R.P., Eds., Society of Automotive Engineers, Warrendale, PA, 1991.
7. Akse, J.R., J. Thompson, B. Scott, C.D. Jolly, and D.L. Carter, Catalytic Oxidation for Treatment of ECLSS and PMMS Waste Streams, *SAE Trans., J. Aerospace*, 101, 910 - 925, 1992.
8. Akse, J.R. and J.E. Atwater, Advanced Catalytic Methods for the Destruction of Environmental Contaminants, Paper No. 95-LS-70, presented at AIAA Life Sciences and Space Medicine Conference '95, Houston, April 3-5, 1995.
9. Carrasquillo, R.L., Status of the Node 3 Regenerative ECLSS Water Recovery and Oxygen Generation System, SAE Technical Paper Series 2003-01-2590, presented at the 33rd International Conference on Environmental Systems, Vancouver, B.C., 2003.
10. Holder, D.W., E.W. O'Connor, J. Zagaja, and K. Murdoch, Investigation into the Performance of Membrane Separator Technologies used in the International Space Station Regenerative Life

Support Systems: Results and Lessons Learned, SAE Technical Paper Series 2001-01-2354, presented at the 31st International Conference on Environmental Systems, Orlando, 2001.
11. Kunetz, J. and L. Hench, Restricted Diffusion of Chromium Nitrate Salt Solutions into Porous Sol-Gel Silica Monoliths, *J. Am. Ceram. Soc.*, 81, 877-884, 1998.
12. Atwater, J.E., J.R. Akse, T.-C. Wang, S. Kimura, and D.C. Johnson, Preparation of Silicon Carbide Coated Activated Carbon Using a High Temperature Fluidized Bed Reactor, *Chem. Eng. Sci.*, 56 (8), 2685-2693, 2001.
13. Levenspiel, O., *Chemical Reaction Engineering*, 2nd Ed., Wiley, New York, 1972.
14. Levenspiel, O., *The Chemical Reactor Omnibook*, Oregon State University, Corvallis, 1979.
15. Froment, G.F., and K.B. Bischoff, *Chemical Reactor Analysis and Design*, 2nd Ed., Wiley, New York, 1990.
16. Boudart, M., and G. Djega-Marriadassou, *Kinetics of Heterogeneous Catalytic Reactors*, Princeton, New Jersey, 1984.
17. Butt, J.B., *Reaction Kinetics and Reactor Design*, Prentice-Hall, Englewood Cliffs, 1980.
18. Hunter, W.G., and R. Mezaki, A Model Building Technique for Chemical Engineering Kinetics, *AIChE J.*, 10, 315, 1964.
19. Barrett, E.P., L.G. Joyner, and P.P. Halenda, The Determination of Pore Volume and Area Distributions in Porous Substances. I. Computations from Nitrogen Isotherms, *J. Am. Chem. Soc.*; 73(1); 373-380,1951.
20. Kresge, C.T., M.E. Leonowicz, W.J. Roth, J.C. Vartuli, and J.S. Beck, Ordered Mesoporous Molecular Sieves Synthesized by a Liquid-Crystal Template Mechanism, *Nature*, 359, 710-712, 1992.
21. Huo, Q., D.I. Margolese, and G.D. Stucky, Surfactant Control of Phases in the Synthesis of Mesoporous Silica-Based Materials, *Chem. Mater.*, 8, 1147-1160, 1996.
22. Zhao, D., P. Yang, D. Margolese, B.F. Chmelka, and G.D. Stucky, Synthesis Of Continuous Mesoporous Silica Thin Films with Three-Dimensional Accessible Pore Structure, *Chem. Commum.*, 22, 2499-2500, 1998.
23. Kramer, E., S. Forster, C. Goltner, and M. Antonietti, Synthesis of Nanoporous Silica with New Pore Morphologies by Templating the Assemblies of Ionic Block Copolymers, *Langmuir*, 14, 2027-2031, 1998.
24. Margolese, D.I., J.A. Melero, S.C. Christiansen, B.F. Chmelka, and G.D. Stucky, Direct Syntheses of Ordered SBA-15 Mesoporous Silica Containing Sulfonic Acid Groups, *Chem. Mater.*, 12, 2448-2459, 2000.
25. Schmidt-Winkel, P., W. Lukens, Jr., P. Yang, D.I. Margolese, J.S. Lettow, J.Y. Ying, and G.D. Stucky, Microemulsion Templating of Siliceous Mesostructured Cellular Foams with Well-Defined Ultralarge Pores, *Chem. Mater.*, 12, 686-696, 2000.
26. Schmidt-Winkel, P., W.W. Lukens, Jr., D. Zhao, P. Yang, B.F. Chmelka, and G.D. Stucky, Mesocellular Siliceous Foams with Uniformly Sized Cells and Windows, *J. Am. Chem. Soc.*, 121, 254-255, 1999.
27. Schmidt-Winkel, P., C.J. Glinka, and G.D. Stucky, Microemulsion Templates for Mesoporous Silica, *Langmuir*, 16, 356-361, 2000.
28. Zhao, D., Q. Huo, J. Feng, B.F. Chmelka, and G.D. Stucky, Nonionic Triblock and Star Diblock Copolymer and Oligomeric Surfactant Syntheses of Highly Ordered, Hydrothermally Stable, Mesoporous Silica Structures, *J. Am. Chem. Soc.*, 120, 6024-6036, 1998.
29. Lettow, J.S., Y.J. Han, P. Schmidt-Winkel, P. Yang, D. Zhao, G.D. Stucky, and J.Y. Ying, Hexagonal to Mesocellular Foam Phase Transition in Polymer-Templated Mesoporous Silicas, *Langmuir*, 16, 8291-8295, 2000.
30. Yang, P., D. Zhao, D. Margolese, B.F. Chmelka, and G.D. Stucky, Generalized Syntheses of Large-Pore Mesoporous Metal Oxides with Semicrystalline Frameworks, *Nature*, 396, 152-155, 1998.
31. Chan, V.Z.-H., J. Hoffman, V.Y. Lee, H. Iatrou, A. Avgeropoulos, N. Hadjichristidis, R.D. Miller, and E.L. Thomas, Ordered Bicontinuous Nanoporous and Nanorelief Ceramic Films form Self Assembling Polymer Precursors, *Science*, 286, 1716-1719, 1999.
32. Anderson, M.T., J.E. Martin, J.G. Odinek, P.P. Newcomer, and J.P. Wilcoxon, Monolithic Periodic Mesoporous Silica Gels, *Microporous Mater.* 10, 13-24, 1997.
33. Zarur, A.J. and J.Y. Ying, Reverse Microemulsion Synthesis of Nanostructured Complex Oxides for Catalytic Combustion, *Nature*, 403, 65-67, 2000.
34. Bagshaw, S.A. and T.J. Pinnavaia, Mesoporous Alumina Molecular Sieves, *Angew. Chem. Int. Edn. Engl.*, 35, 1102-1105, 1996.
35. Forster, S., and D.M. Antonietti, Amphiphilic Block Copolymers in Structure-Controlled Nanomaterials Hybrids, *Adv. Mater.*, 10, 195-217. 1998.
36. Antonietti, D.M., and J.Y. Ying, Synthesis and Characterization of Hexagonal Packed Mesoporous Tantalum Oxide Molecular Sieves, *Chem. Mater.*, 8, 874-881, 1996.
37. Antonietti, D.M., and J.Y. Ying, Synthesis of Hexagonal Packed Mesoporous TiO_2 by a Modified Sol-Gel Method, *Angew. Chem. Int. Edn. Engl.*, 34, 2014-2017, 1995.
38. Wright, J.D. and N. Sommerdijk, *Sol-Gel Materials; Chemistry and Applications*, Gordon and Breach Publishers, 2001.
39. Takahashi, R, S. Sato, T. Sodesawa, and K. Suzuki, Phase Separation in Sol-Gel process of Alkoxide-Derived Silica-Zirconia in the Presence of Polyethylene Oxide, *J. Am. Ceram. Soc.*, 84, 1968-1976, 2001.
40. Wong, M.S., H.C. Huang, and J.Y. Ying, Supramolecular-Templated Synthesis of Nanoporous Zirconia-Silica Catalysts, *Chem. Mater.*, 14, 1961-1973, 2002.

41. Zhang, Z., R.W. Hicks, T.R. Pauly, and T.J. Pinnavaia, Mesostructured Forms of γ-Al_2O_3, *J. Am. Chem. Soc.*, 124, 1592-1593, 2002.
42. Mokaya, R. and W. Jones, Aluminosilicate Mesoporous Molecular Sieves with Enhanced Stability Obtained by reacting MCM-41 with Aluminum Chlorohydrate, *Chem. Commun.*, 1839-1840, 1998.
43. Mokaya, R. and W. Jones, Efficient Post-synthesis Alumination of MCM-41 using Aluminum Chlorohydrate Containing Al Polycations, *J. Mater. Chem.*, 9, 555-561, 1999.
44. Atwater, J.E., J.R. Akse, T.-C. Wang, J.M. Rodarte, J.A. Hurley, and J.O. Thompson, Silicon Carbide Coated Granular Activated Carbon: a Robust Support for Low Temperature Aqueous Phase Oxidation Catalysts. *Carbon*, 35, 1678-1679, 1997.
45. Atwater, J.E., J.R. Akse, J.A. McKinnis, and J.O. Thompson, Low Temperature Aqueous Phase Catalytic Oxidation of Phenol, *Chemosphere*, 34 (1), 203-212, 1997.
46. Atwater, J.E., J.R. Akse, J.A. McKinnis, and J.O. Thompson, Aqueous Phase Heterogeneous Catalytic Oxidation of Trichloroethylene, *Appl. Catal. B.*., 11, L11-L18, 1996.
47. Akse, J.R., J.E. Atwater, J.A. McKinnis, J.O. Thompson, and J.A. Hurley, Elimination of Organic Contaminants in Wastewater using Molecular Oxygen and the Aqueous Phase Catalytic Oxidation Process, Seventh International Chemical Oxidation Symposium, Nashville, TN, April 9-11, 1997.
48. Press, W.H., B.P. Flannery, S.A. Teukolsky, and W.T. Vetterling, *Numerical Recipes: The Art of Scientific Computing*, Cambridge, New York, 1986.
49. Brunauer, S., P.H. Emmett, and E. Teller, Adsorption of Gases in Multimolecular Layers, *J. Amer. Chem Soc.*, 60, 309, 1938.
50. Gregg, S.J. and K.S.W. Sing, *Adsorption Surface Area and Porosity*, Academic Press, New York, 1967.